



Palladium on graphene as efficient catalyst for solvent-free aerobic oxidation of aromatic alcohols: Role of graphene support



Guangjun Wu, Xueming Wang, Naijia Guan, Landong Li*

Key Laboratory of Advanced Energy Materials Chemistry (Ministry of Education), College of Chemistry, Nankai University, Tianjin 300071, PR China

ARTICLE INFO

Article history:

Received 24 October 2012

Received in revised form

27 December 2012

Accepted 27 January 2013

Available online 14 February 2013

Keywords:

Pd catalysts

Graphene

Aerobic oxidation

Aromatic alcohols

ABSTRACT

Palladium catalysts supported on different carbon materials, i.e. graphene, carbon nanotube and activated carbon, have been prepared by improved wet impregnation and employed in the solvent-free aerobic oxidation of aromatic alcohols using molecular oxygen as oxidant. High catalytic activity as well as high selectivity to corresponding carbonyl compounds can be obtained on Pd/graphene. Typically, an extremely high turnover frequency of 30,137 mol/h mol_{Pd} is observed in the aerobic oxidation of benzyl alcohol to benzaldehyde using Pd/graphene as catalyst. Palladium catalysts on different carbon supports are fully characterized by a series of techniques, e.g. Raman, XRD, SEM, TEM, TG, XPS, FTIR spectra of benzyl alcohol adsorption and O₂-TPD. Based on the catalytic and characterization results, the superior reactivity of Pd/graphene in the aerobic oxidation of aromatic alcohols is attributed to the promotion role of graphene support in the adsorption of reactant alcohol and oxygen.

© 2013 Elsevier B.V. All rights reserved.

1. Introduction

The selective oxidation of alcohols to corresponding carbonyl compounds, e.g. aldehydes or ketones, is one of the most useful and fundamental transformations in organic synthesis [1]. With environmental and economic concerns, heterogeneous catalysis reaction using molecular oxygen as primary oxidant is developed as desired green process for alcohol selective oxidation [2,3]. Up to now, numerous catalyst systems have been explored and palladium catalysts receive special attentions due to their high activity as well as high selectivity [4–19]. Palladium catalysts on different supports, e.g. Pd/hydroxyapatite [4], Pd/Al₂O₃ [7–9], Pd/carbon [10,16], Pd/MgO [5,17] and Pd/mesoporous silica [14,18], have been successfully applied in the aerobic selective oxidation of various alcohols under different reaction conditions. As for supported palladium catalysts, the properties of support materials may greatly influence the resulting catalytic activities from different perspectives. On the one hand, the supports may influence the existence states, e.g. particle sizes and electronic structure, of catalytically-active palladium clusters through metal–support interaction, and therefore, shows indirect impacts on the catalytic activities. On the other hand, the physico-chemical properties of supports may influence the adsorption and mass transport of reaction substrate, and therefore, show direct impacts on the catalytic reaction. Undoubtedly, the comprehensive understanding

of support effects makes great sense for the design of highly-active palladium catalysts for the aerobic selective alcohol oxidation.

Carbon materials are commonly used as catalyst supports for noble metals due to several advantages, e.g. high surface area, good chemical stability and easy recovery of noble metals from spent catalysts [20]. Specifically, Pd/C is recognized as a model heterogeneous catalyst for the selective hydrogenation and selective oxidation. Graphene, a two-dimensional sheet of sp²-hybridized carbon, has become one of the most intriguing research topics since its first experimental isolation in 2004 [21–24]. All the structural, electrical and physical properties make graphene an ideal support material for noble metal nanoparticles. The integrated cost reduction for graphene production has been achieved with the emerging of new synthesis strategies [25,26], and accordingly, the large-scale use of graphene as support can be expected. In fact, graphene has been widely used as support material and a variety of graphene supported noble metal nanoparticles have been developed for various catalytic applications [27]. Typically, graphene supported palladium nanoparticles have been reported to be efficient catalysts for several reactions, e.g. carbon–carbon cross-coupling reaction [28–31], ammonia borane dehydrogenation [32] and CO oxidation [33,34]. In these cases, the high activity of Pd/graphene is primarily attributed to the high dispersion and small particle size of palladium nanoparticles on graphene [29–33]. However, in our opinion, the properties of graphene support should influence the catalytic activity of Pd/graphene in multiple aspects, not only limited to the effects on the dispersion and size of catalytically-active palladium nanoparticles.

* Corresponding author. Tel.: +86 22 2350 0341; fax: +86 22 2350 0341.

E-mail address: lild@nankai.edu.cn (L. Li).

In the present study, palladium catalysts supported on different carbon materials are explored as catalysts for the selective oxidation of aromatic alcohols in liquid-phase via ideal green process, i.e. using molecular oxygen as oxidant and be free of any solvent or additives. Palladium on graphene will be developed as efficient catalyst for the aerobic oxidation of aromatic alcohols to corresponding carbonyl compounds. The role of graphene support on the catalytic activity of Pd/graphene will be discussed in detail.

2. Experimental

2.1. Sample preparation

Carbon nanotube (CNT, BET surface area: 352 m²/g), activated carbon (AC, BET surface area: 497 m²/g), graphite powder (99.9999% metals basis), and reference activated carbon supported palladium catalyst (denoted as Pd/AC-ref, 5% Pd, BET surface area: 458 m²/g) were purchased from Alfa Aesar. Graphene oxide was synthesized from graphite based on the method developed by the Hummers and co-workers [35]. Briefly, graphite was oxidized by treating with KMnO₄ and NaNO₃ in concentrated H₂SO₄ to form graphite oxide, and the obtained graphite oxide was exfoliated into graphene oxide (GO) by ultrasonication in aqueous mediate. The GO was purified by configuration and dialysis to remove the impurities, dried at ambient conditions, and calcined in flowing He at 573 K for 4 h to obtain chemically derived graphene (denoted as GC).

Palladium species were introduced to different carbon supports (GC, CNT and AC) by wet impregnation method using PdCl₂ as precursor [36]. In a typical preparation process of Pd/GC, 1 mL PdCl₂ solution in acetone (Pd concentration: 1.5 mg/mL) was added drop-wised to 200 mg GC with vigorous agitation and then dispersed in ultrasonication for 30 min. After drying at ambient conditions, the as-obtained sample was treated in flowing He at 573 K for 1 h and then reduced in flowing 10% H₂/He at 573 K for 1 h. For reference, Pd catalyst supported on GO, i.e. Pd/GO, was prepared by chemical reduction method. In the chemical reduction process, GO and PdCl₂ solution were added into distilled water and dispersed by ultrasonic vibration for 30 min. Palladium ions were reduced by the addition of sufficient 1 mol/L KBH₄ under the protection of nitrogen. The resulting suspension was filtered, washed by distilled water and dried at ambient conditions.

2.2. Sample characterization

The palladium loadings in palladium catalysts supported on different carbon materials were analyzed on a Perkin Elmer Optima 2000 inductively coupled plasma optical emission spectrometer (ICP-OES).

Raman spectra of grapheme-based materials were recorded on a Renishaw InVia Raman spectrometer with the green line of an Ar-ion laser (514.5 nm) in micro-Raman configuration.

X-ray diffraction (XRD) patterns of the samples were recorded on a Bruker D8 diffractometer with CuK α radiation ($\lambda = 0.1542$ nm) from 10–80° with a scan speed of $2\theta = 6.0^\circ/\text{min}$.

Nitrogen adsorption/desorption of the samples were measured at 77 K on Quantachrome iQ-MP gas absorption analyzer after out-gassing at 473 K under vacuum for 12 h. The specific surface area was calculated with the Brunauer–Emmett–Teller (BET) equation.

Transmission electron microscopy (TEM) images of the samples were acquired on a Tecnai G2 F20 U-TWIN transmission electron microscope at an acceleration voltage of 200 kV. A few drops of alcohol suspension containing the catalyst samples were placed on a micro grid, followed by evaporation at ambient temperature. Scanning electron microscopy (SEM) images of the samples were acquired on JEOL-JSM7500 scanning electron microscope.

Thermogravimetric analysis (TGA) of the samples was performed on a Rigaku standard type thermogravimetric analyzer. In a typical measurement, 0.1 g of the sample was heated in an Al₂O₃ crucible with a constant heating rate of 10 K/min and under He purging using a flow rate of 25 mL/min.

The temperature-programmed desorption of oxygen (O₂-TPD) on palladium catalysts supported on different carbon materials was performed on the chemisorption analyzer. The samples were pre-treated in 10%O₂/He at 473 K for 2 h and then cooled down to room temperature in the same flow. After He purge for 30 min at 323 K, the temperature-programmed desorption experiments were conducted in He flow from 323 to 873 K at a heating rate of 10 K/min.

X-ray photoelectron spectra (XPS) of the samples were recorded on a Kratos Axis Ultra DLD spectrometer with a monochromated Al-K α X-ray source ($h\nu = 1486.6$ eV), hybrid (magnetic/electrostatic) optics and a multi-channel plate and delay line detector (DLD). The high-resolution spectra were recorded with pass energy of 40 eV using an aperture slot of 300 $\mu \times 700 \mu$. Accurate binding energies (± 0.1 eV) were determined with respect to the position of the adventitious C 1s peak at 284.8 eV.

FTIR spectra of benzyl alcohol adsorption on samples were collected on the Bruker Tensor 27 spectrometer with 128 scans at a resolution of 4 cm⁻¹. A self-supporting pellet made of the catalyst sample was placed in the IR flow cell and the background spectrum was taken at 383 K. Benzyl alcohol was introduced to the samples by flowing He and FTIR spectra of benzyl alcohol adsorption on the samples were recorded at 383 K after time-on-stream of 1 h.

2.3. Aerobic oxidation of aromatic alcohols

The solvent-free aerobic oxidation of aromatic alcohols over palladium catalysts supported on different carbon materials was performed under atmosphere pressure. In each experiment, 15 mg of the catalyst sample was dispersed in 0.24 mol corresponding aromatic alcohol in a three-necked batch reactor with a reflux condenser under stirring of 1000 rpm/min. The suspension was kept at 383 K with oxygen bubbled in at a flow-rate 20 mL/min. After the reaction, the catalyst sample was removed from the reaction mixture by centrifugation and the products were analyzed by gas chromatography (Shimadzu GC-2010 Plus, flame ionisation detector, He carrier and 30 m DB-FFAP capillary column with program: isothermal at 423 K for 10 min and then heated to 473 K at a ramping rate of 10 K/min) as well as GC-MS (Shimadzu GCMS-QP2010 SE). The carbon balance in liquid phase is found to be >95% for all tests, and therefore, the formation of volatile products, e.g. CO and CO₂, is neglected.

3. Results and discussion

3.1. Characterization of palladium catalysts supported on different carbon materials

Raman spectroscopy is a very useful tool to characterize graphene-based materials, and the Raman spectra of as-prepared graphene oxide, GC and Pd/GC are shown in Fig. 1. The exfoliated graphene oxide shows a strong disorder-induced D band and an in-plane vibration of the graphene lattice G band at 1345 and 1590 cm⁻¹, respectively, and their overtones (2D, D+G and 2G) at 2500–3300 cm⁻¹ [37]. The chemically derived GC also shows similar D and G bands at 1345 and 1590 cm⁻¹, respectively. The intensity ratio D-band to G-band, i.e. I_D/I_G , has been used to measure the quality of the graphitic structure and the value of I_D/I_G is approaching zero for defect-free graphene [38]. While in the present study, high I_D/I_G value of ca. 1.2 is observed for as-prepared GC, indicating the existence of abundant surface defects. The

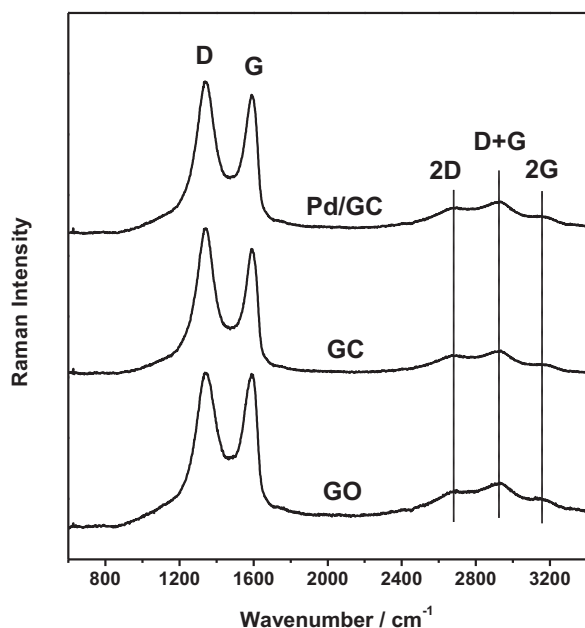


Fig. 1. Raman spectra of GO, GC and Pd/GC.

introduction of palladium species to GC does not cause obvious change in the value of I_D/I_G , due to the low palladium loading. According to the reports of El-Shall et al. [30], the structure defects in GC may play an important role in enhancing the catalytic activity of Pd/GC sample although the defects are undesirable for electronic applications. On a whole, the results from Raman spectra confirm that graphene oxide and GC are successfully prepared in this study, and the typical structure of GC with structure defects is preserved after the introduction of palladium species.

Fig. 2 shows the XRD patterns of Pd/GC, Pd/AC, Pd/CNT and Pd/AC-ref. Typical diffraction peaks corresponding to support carbon materials, i.e. GC (002) at 25.9° , CNT (100), (002) and (004) at 44.5 , 26.5 and 51.9° respectively, and AC (002) at 25.0° [39–41], are observed in supported palladium catalysts. Besides, diffraction peaks at 40.2 , 46.5 and 68.0° corresponding to the (111), (200) and (220) planes of a face-centered cubic lattice of metallic palladium

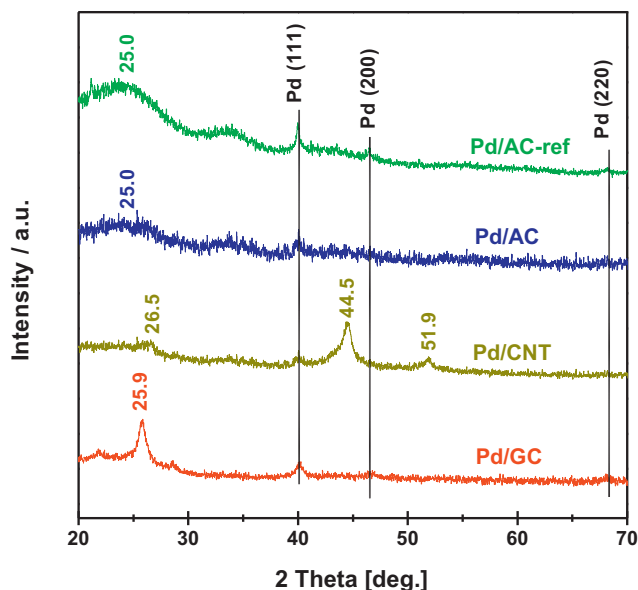


Fig. 2. XRD patterns of Pd/GC, Pd/AC, Pd/CNT and Pd/AC-ref.

(JCPDS 46-1043) can be observed, indicating that the palladium species exist in the metallic form on various carbon supports.

Fig. 3 shows the SEM and TEM images of Pd/GC, Pd/AC and Pd/CNT. The sheet morphology with typical wrinkle of GC is clearly observed in the TEM and SEM images of Pd/GC. The typical nanotube structure of CNT is observed in the TEM image of Pd/CNT, while bulk aggregates of sample are observed in the SEM image of Pd/CNT. From the TEM images of palladium catalysts, uniform palladium nanoparticles are observed to disperse on different carbon supports. The sizes of palladium nanoparticles are quite similar, with little relation to the properties of supports. Typically, the mean size of palladium nanoparticle is observed to be 4.1 nm on GC, 3.8 nm on CNT and 4.3 nm on AC (Table 1).

The thermal stability of palladium catalysts supported on different carbon materials are examined by means of TGA, and the results are shown in Fig. 4. It is seen that all samples exhibit continuous weight loss from 300 to 1100 K. The weight loss below 373 K should be due to the deintercalation of H_2O from samples, while the weight loss above 373 K should be mainly due to the decomposition of surface oxygen-containing functional groups from carbon supports [42]. The weight loss of >10% of all samples are observed above 373 K, indicating the existence of abundant surface oxygen-containing functional groups on carbon supports. In the temperature range of 373–673 K, a relatively small weight loss of 2.5% is observed on Pd/GC, in great contrast to the big weight loss of 7.4 and 9.3% on Pd/CNT and Pd/AC, respectively. It is thus indicated that the surface oxygen-containing functional groups on GC are thermally more stable than those on CNT and AC. These surface oxygen-containing functional groups might play an important role in stabilizing palladium species and promoting the adsorption of alcohol reactant (vide infra).

The chemical composition and surface functional groups of palladium catalysts supported on different carbon materials are investigated by means of XPS, and the results are shown in Fig. 5. In the C 1s region, the binding energy peaks at 284.6, 285.7 and 287.1 eV are observed for all samples, corresponding to graphitic C–C, C–O and C=O groups, respectively [43–45]. For Pd/GC, additional C 1s binding energy peak at 290.1 eV corresponding to O–C=O groups can be observed [45]. In the O 1s region, the binding energy peaks at 531.5 and 532.7 eV are observed for all samples, corresponding to C=O and C–O groups, respectively [46]. For Pd/GC, additional O 1s binding energy peak at 533.9 eV corresponding to O–C=O groups can be observed [47]. The XPS results clearly indicate the existence of oxygen-containing groups in palladium catalysts supported on different carbon materials, in consistent with TGA results. Specifically, C=O and C–O groups exist in all samples, while O–C=O groups only exist in Pd/GC. The percentages of total oxygen-containing groups are estimated to be over 20% for all samples based on the deconvolution of C 1s peaks, and these groups should locate at the defect sites in carbon supports. In the Pd 3d region, the binding energy peaks at 335.4 and 340.6 eV are observed for all samples, corresponding to the Pd $3d_{5/2}$ and Pd $3d_{3/2}$, respectively [48]. Based on the Pd 3d XPS results, palladium species exist in the metallic form in all samples after reduction treatment, and no obvious differences in the electronic states of palladium can be observed for palladium catalysts supported on different carbon supports.

The adsorption of reactant alcohol on catalyst is an important step for subsequent aerobic oxidation reaction. In the present study, the adsorption of benzyl alcohol on palladium catalysts supported on different carbon materials is investigated by means of FTIR spectroscopy. As shown in Fig. 6, benzyl alcohol adsorption on samples results in the appearance of a series of IR bands. Typically, the bands at 1600, 1585, 1495 and 1455 cm^{-1} are attributed to the benzene skeleton vibrations ν_{C-C} in benzyl alcohol (benzene skeleton C–H deformation vibration at 700 cm^{-1}), while the band at 1015 cm^{-1}

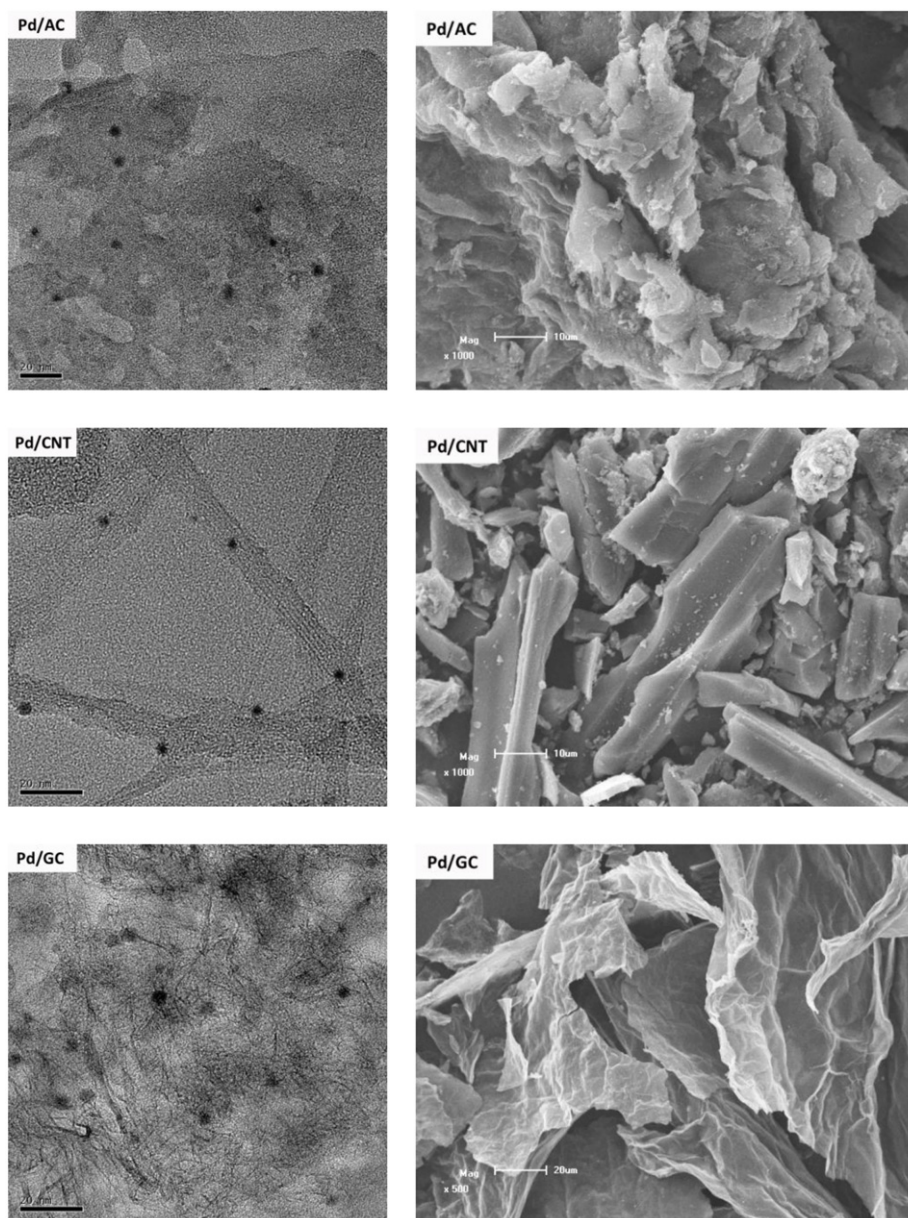


Fig. 3. TEM (left) and SEM (right) images of Pd/GC, Pd/AC and Pd/CNT.

Table 1
Benzyl alcohol oxidation over palladium catalysts on different carbon supports.^a

Catalyst	Surface area (m ² /g)	Pd loading (%)	Pd size (nm) ^b	Conversion (%) ^c	Yield (%) ^d	TOF ^e (mol/h mol _{Pd})
GC	786	0	/	0.6	0.5	/
CNT	352	0	/	0.3	0.3	/
AC	497	0	/	0.4	0.4	/
Pd/GC	765	0.68	4.1	72.5	70.2	30,137
Pd/GC ^f	738	0.66	4.1	71.6	68.9	29,747
Pd/GC ^g	741	0.67	4.1	71.8	69.1	29,846
Pd/GO	304	0.69	4.9	36.2	34.1	15,017
Pd/CNT	389	0.72	3.8	17.6	16.3	6910
Pd/AC	416	0.71	4.3	28.7	25.3	11,267
Pd/AC-ref	458	4.92	6.2	48.8	45.9	2803

^a Reaction conditions: 15 mg catalyst, 0.24 mol benzyl alcohol, 383 K.

^b Average size observed by TEM.

^c Benzyl alcohol conversion at time-on-stream of 6 h.

^d Yield of benzaldehyde at time-on-stream of 6 h.

^e Calculated as the ratio of moles of alcohol converted per mole of total Pd per hour.

^f Second use of Pd/GC.

^g Third use of Pd/GC.

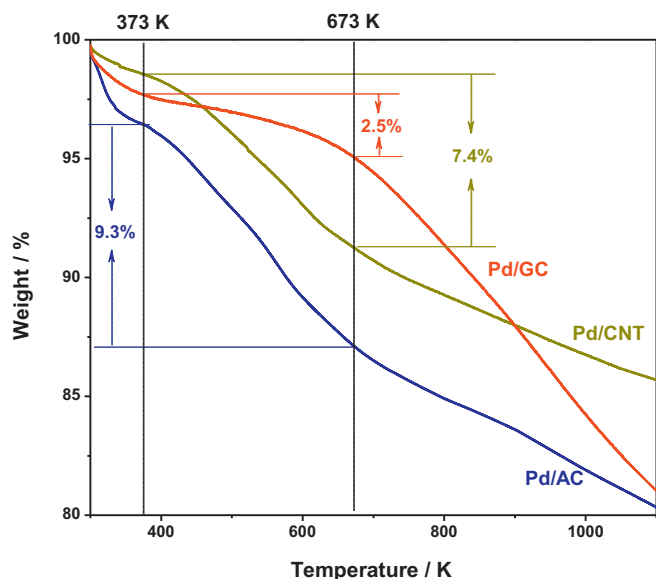


Fig. 4. TGA curves of Pd/GC, Pd/AC and Pd/CNT.

is attributed to the C–O stretching vibration $\nu_{\text{C-O}}$ in benzyl alcohol [49]. Obviously, two major types of benzyl alcohol adsorption can be distinguished: benzene skeleton adsorption and hydroxyl adsorption. Based on FTIR spectra, the adsorption capacity toward benzyl alcohol is observed to be Pd/GC > Pd/AC > Pd/CNT. Especially, the benzene skeleton adsorption on Pd/GC is much higher than that on Pd/AC and Pd/CNT. This should be due to the formation of π -electron interaction between benzene skeleton and graphene, which distinctly promotes the adsorption of benzyl alcohol on Pd/GC.

The adsorption of oxygen on different palladium catalysts is investigated by means of O_2 -TPD. As shown in Fig. 7, oxygen desorption peak below 450 K can be observed for all samples, corresponding to the desorption of most energetically labile oxygen species on palladium sites [50]. The intensity of oxygen desorption peak is rather low on Pd/AC and Pd/CNT, probably due to the low palladium loadings. While for Pd/GC, the intensity of oxygen desorption peak is much higher. It has been proposed that oxygen

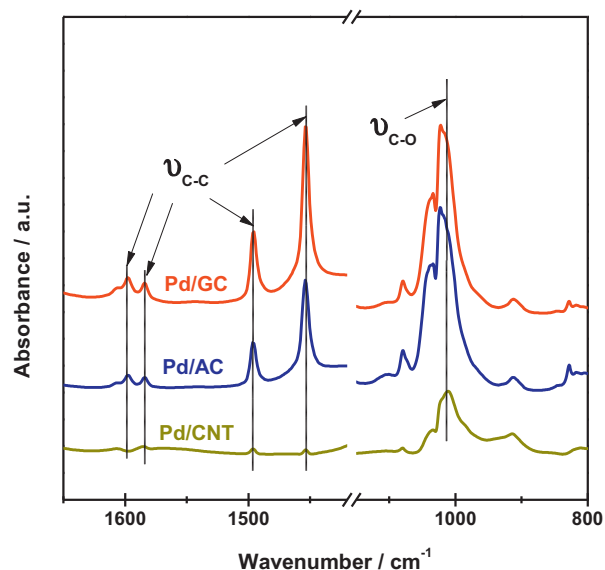


Fig. 6. O_2 -TPD profiles of Pd/GC, Pd/AC and Pd/CNT.

can adsorb on the bridge sites of graphene with migration energy of over 1.0 eV [51]. Therefore, oxygen can adsorb on the palladium sites and then spill over to the adjacent bridge sites of graphene. In such a way, the adsorption of oxygen on Pd/GC is greatly promoted.

3.2. Aerobic oxidation of aromatic alcohols on palladium catalysts

The time-dependent benzyl alcohol aerobic oxidation catalyzed by palladium on different carbon supports is shown in Fig. 8. For all catalysts, benzyl alcohol conversions increase linearly with prolonged reaction time up to 8 h. The major product is benzaldehyde (>90%), and small quantities of benzoic acid (from the over-oxidation of product benzaldehyde) and benzylbenzoate (from the esterification between benzyl alcohol and benzoic acid) are detected as by-products. The leaching of palladium in liquid phase cannot be detected in all catalytic tests (the reaction system was diluted with 20 mL methanol and Pd catalysts after reaction were separated from solution by high-speed centrifugation. The Pd

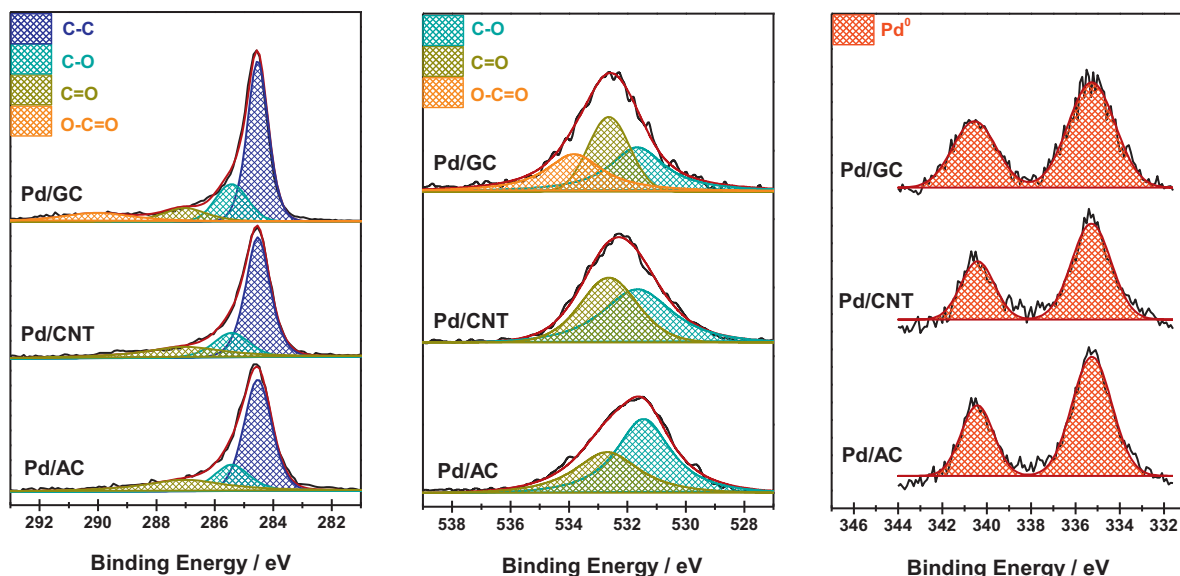


Fig. 5. XPS of C1s, O1s and Pd 3d region of Pd/GC, Pd/AC and Pd/CNT.

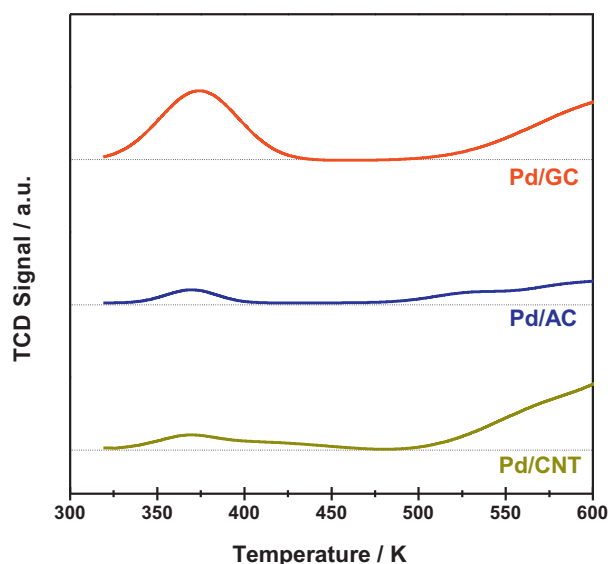


Fig. 7. FTIR spectra of benzyl alcohol adsorption on Pd/GC, Pd/AC and Pd/CNT.

loading in solution was below the detection limit of ICP), and therefore, the activity contribution from leached palladium complex can be neglected. Carbon supports show very low activity (<1%) in the aerobic oxidation of benzyl alcohol (Table 1), and activity contribution from carbon supports can also be neglected. With similar palladium loading, Pd/GC exhibits the highest activity for benzyl alcohol aerobic oxidation, followed by Pd/AC and then Pd/CNT. Pd/GC with very low palladium loading of 0.68% even shows distinct higher activity than commercial Pd/AC-ref with high palladium loading of 5.92%. The superior benzyl alcohol oxidation activity of Pd/GC is further revealed by its extremely high TOF of 30,137 mol/h mol_{Pd}, which is >10 times higher than that of commercial Pd/AC-ref. Moreover, Pd/GC shows much higher activity in benzyl alcohol oxidation than Pd/GO, revealing the unique properties of GC as catalyst support.

The Pd/GC catalyst after benzyl alcohol aerobic oxidation can be separated from the reaction mixture by simple centrifugation

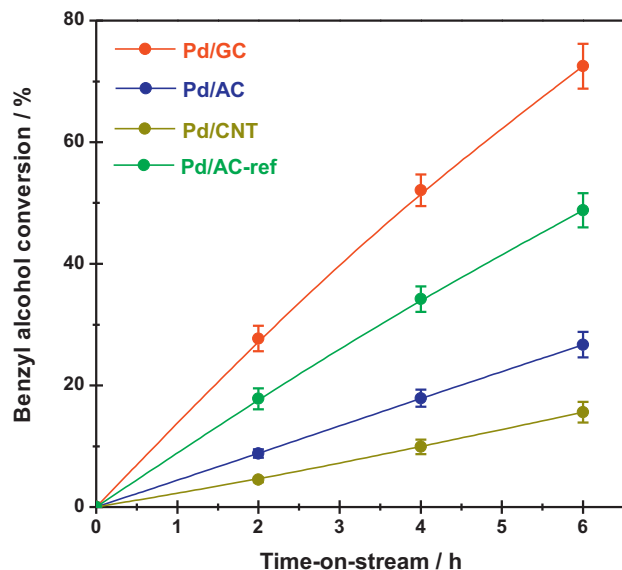


Fig. 8. Selective oxidation of benzyl alcohol over Pd/GC, Pd/AC, Pd/CNT and Pd/AC-ref at 383 K.

and the regeneration of Pd/GC can be accomplished by vacuum desiccation at 373 K for 2 h. The regenerated Pd/GC shows quite similar benzyl alcohol oxidation activity to the fresh catalyst, as shown in Table 1. The good recyclability of Pd/GC demonstrates its potential as promising heterogeneous catalyst for aerobic oxidation reaction. To have a better understanding on its good recyclability, Pd/GC catalysts after benzyl alcohol oxidation are further analyzed by TEM and XPS. The TEM images in Fig. 9 clearly indicate that the size of palladium clusters on GC is kept nearly unchanged after benzyl alcohol oxidation and therefore the catalytic deactivation induced by the agglomeration of active palladium species could be completely avoided. For as-prepared Pd/GC, metallic palladium (binding energy at 335.2 and 340.6 eV) is observed as the exclusive palladium species. After reaction of benzyl alcohol oxidation (first use), predominant metallic palladium species (binding energy at 335.2 and 340.6 eV) as well as a small part of hydrated or coordinated Pd²⁺ species (binding energy at 337.2 and 342.5 eV) [52] can be observed for Pd/GC. It is evident that some of metallic palladium can be oxidized to Pd²⁺ during benzyl alcohol oxidation under our reaction conditions. However, the small change in the existence state of palladium does not lead to a visible deactivation of Pd/GC (Table 1). The further oxidation of metallic palladium species could not be observed during next reaction and the percentage of Pd²⁺ in overall palladium species estimated from XPS does not increase after the third use. Therefore, a stable existence state of palladium species, i.e. a majority of metallic palladium with a small part of ionic palladium species, can be concluded for Pd/GC after reaction, which is essential for its stable activity and good recyclability in benzyl alcohol oxidation.

Initiated by the superior activity of Pd/GC for the oxidation of benzyl alcohol, we further investigated the aerobic oxidation of various aromatic alcohols catalyzed by Pd/GC under solvent-free conditions. As shown in Table 2, Pd/GC exhibits high catalytic activity for the aerobic oxidation as well as good selectivity to carbonyl compounds in most cases. Exceptionally, the oxidation of diphenylmethanol catalyzed by Pd/GC is very slow because the adsorption of diphenylmethanol onto catalyst is difficult due to steric hindrance. For the aerobic oxidation of para-substituted benzyl alcohols, the catalytic activity is governed by the Hammett rule, i.e. substitution with electron-releasing groups —OCH₃ and —CH₃ increases the activity while substitution with electron-releasing groups —Cl and —NO₂ decreases the activity. In all cases, the catalytic activity of Pd/GC is several times higher than Pd/AC with similar palladium loading, which clearly demonstrates the advantage of GC as support for palladium catalysts. It should be mentioned that ~100% oxidation of primary aromatic alcohols cannot be achieved with the extension of time-on-stream. The successive oxidation of product aldehydes to carboxylic acids and subsequent esterification between alcohols and carboxylic acids cannot be avoided under our reaction conditions. During the aerobic oxidation of benzyl alcohol catalyzed by Pd/GC, the selectivity to benzaldehyde decreases with increasing benzyl alcohol conversion, while the selectivity to benzoic acid and benzyl benzoate increases. After time-on-stream of 24 h, no benzyl alcohol can be detected in the reaction system and ca. 8% non-oxidized benzyl alcohol exists in benzyl benzoate, as shown in Fig. 10. For the aerobic selective oxidation of secondary aromatic alcohols, ketones are detected as the only products and ~100% oxidation of secondary aromatic alcohols is possible. For example, ca. 99% α-phenylethyl alcohol conversion and 99.9% selectivity to acetophenone can be achieved in the oxidation of α-phenylethyl alcohol catalyzed by Pd/GC after time-on-stream of 72 h (Fig. 10). From this point of view, the aerobic selective oxidation of secondary aromatic alcohols to corresponding ketones using Pd/GC as catalyst might be more promising reaction for industrial application.

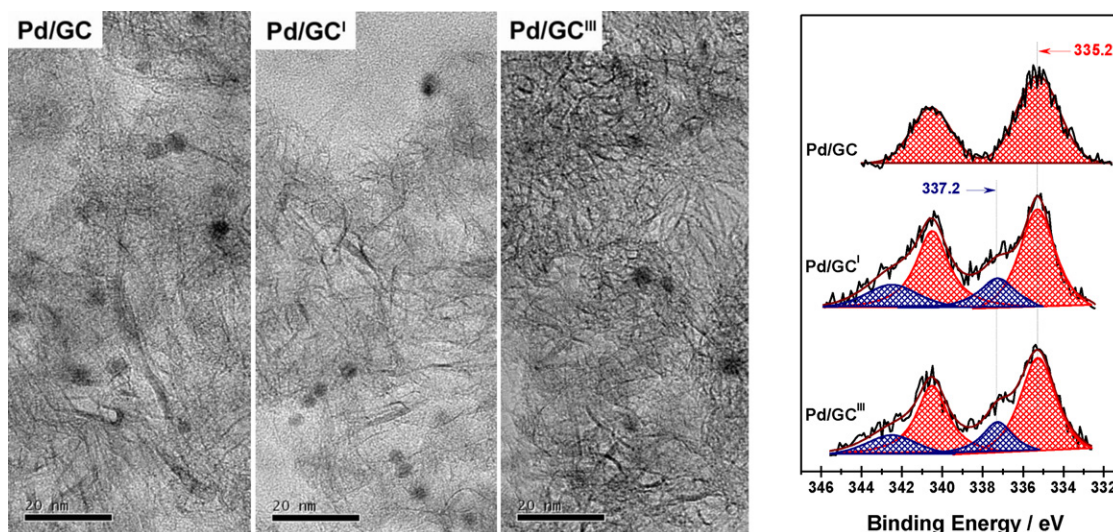


Fig. 9. TEM images and Pd 3d XPS of Pd/GC before and after reaction (Pd/GC^I: Pd/GC after first use; Pd/GC^{III}: Pd/GC after third use).

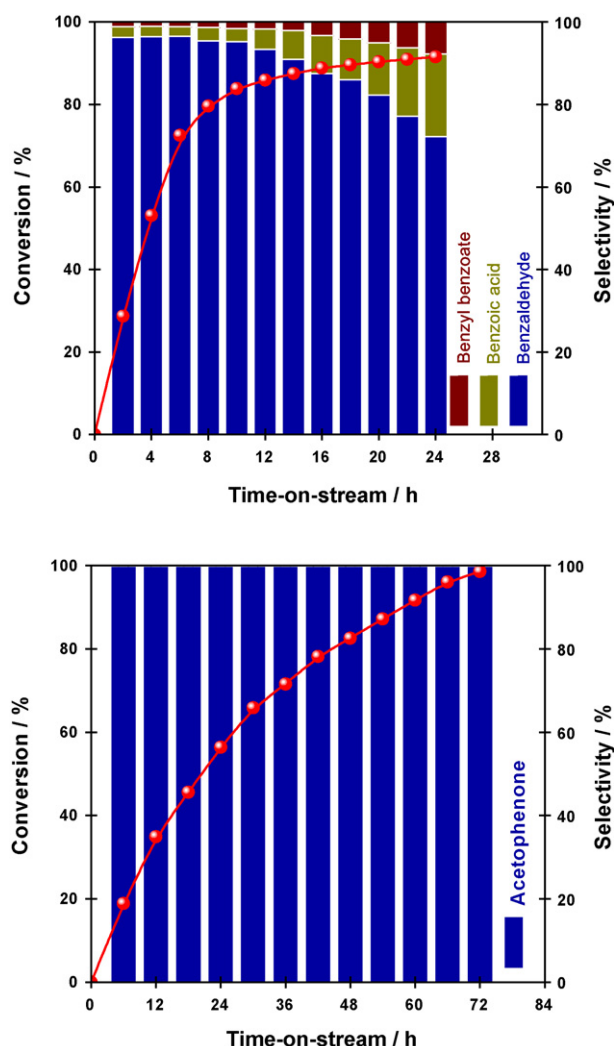
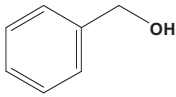
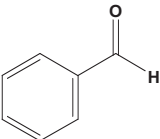
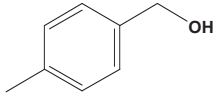
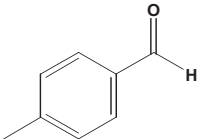
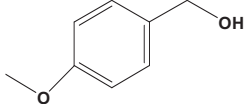
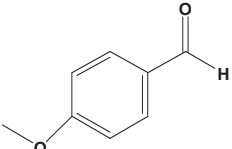
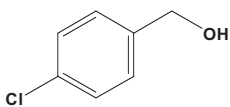
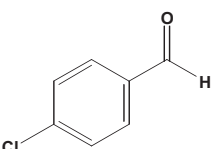
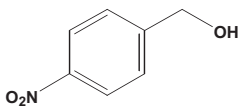
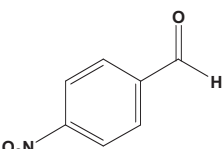
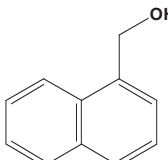
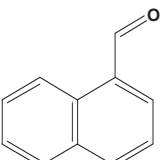
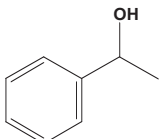
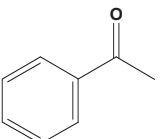
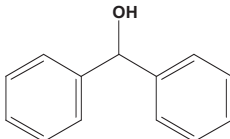
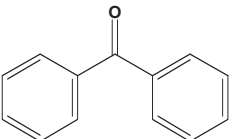


Fig. 10. Time-on-stream behavior of benzyl alcohol and α -phenylethanol oxidation selective oxidation over Pd/GC at 383 K.

3.3. Role of GC support on the activity of palladium catalyst

The support effects on the activity of palladium catalysts for the aerobic oxidation of alcohols have been extensively studied in the past [14–18]. The existence states of catalytically-active palladium sites can be strongly influenced by the physicochemical properties of supports through metal–support interaction. Typically, the size-dependent catalytic activity of supported palladium nanoparticles has been established for the aerobic oxidation of alcohols [11]. In the present study, supported palladium catalysts similar palladium particle sizes (Fig. 3) are applied in the aerobic oxidation of aromatic alcohols and the activity difference caused by the particle sizes can be excluded. The XPS results further confirm that palladium species exist in the similar metallic form on different carbon supports (Fig. 5). Since both the particle sizes and electronic structure of catalytically-active palladium sites are quite similar on different carbon supports, the high activity of Pd/GC should be explained from other aspects, i.e. the adsorption of reactant alcohols and oxygen. The FTIR spectra of benzyl alcohol adsorption in Fig. 6 reveal that Pd/GC exhibits higher adsorption capacity toward benzyl alcohol than Pd/AC and Pd/CNT, due to the formation of π -electron interaction between benzene skeleton and graphene. Undoubtedly, the high adsorption capacity toward reactant alcohol can promote the subsequent aerobic oxidation reaction. It should be mentioned that GC is known as two-dimensional sheet sp^2 -hybridized carbon with unique π -conjugated electron system, and therefore, its promotion effect on the adsorption of alcohol is more obvious for alcohols with π -electron system and quasi-planar structure. From this point of view, aromatic alcohols should be suitable reactant alcohols for aerobic oxidation when using Pd/GC as catalysts. In addition to the promotion effect on alcohol adsorption, the O_2 -TPD profiles indicate that the adsorption of oxygen on Pd/GC is greatly promoted compared to that on Pd/AC and Pd/CNT (Fig. 7), due to oxygen spill-over from palladium sites to the adjacent bridge sites of graphene. It is known that the aerobic oxidation of alcohols may proceed via classical two-step dehydrogenation mechanism [3]. The role of oxygen is to oxidize the co-product hydrogen and thus shift the equilibrium toward the carbonyl compound [53,54]. The existence of mobile oxygen on graphene support can promote the elimination of hydrogen and thus promote the aerobic oxidation of alcohols. On a whole, the use of GC as support for palladium species can promote the adsorption of both reactant aromatic alcohols and oxygen. Accordingly, extremely high activities in the aerobic oxidation of

Table 2
Aerobic oxidation of aromatic alcohols over Pd/GC and Pd/AC.^a

Entry	Substrate	Product	Catalyst	Conversion (%) ^b	Selectivity (%) ^c	TOF ^d (mol/h mol _{Pd})
1			Pd/GC	72.5	98.3	30,137
			Pd/AC	28.7	88.2	11,267
2			Pd/GC	78.2	97.8	32,415
			Pd/AC	35.8	90.3	14,054
3			Pd/GC	80.9	83.2	33,627
			Pd/AC	41.2	82.9	16,175
4			Pd/GC	35.4	95.2	14,717
			Pd/AC	8.1	91.3	3180
5			Pd/GC	16.7	99.1	6943
			Pd/AC	5.1	98.5	2003
6			Pd/GC	79.6	96.4	33,089
			Pd/AC	26.3	91.6	10,324
7			Pd/GC	18.9	>99.9	7856
			Pd/AC	3.2	>99.9	1256
8			Pd/GC	1.6	>99.9	666
			Pd/AC	1.2	>99.9	472

^a Reaction conditions: 15 mg catalyst, 0.24 mol aromatic alcohol, 383 K.

^b Aromatic alcohol conversion at time-on-stream of 6 h.

^c Aldehyde or ketone selectivity at time-on-stream of 6 h.

^d Calculated as the ratio of moles of alcohol converted per mole of total Pd per hour.

aromatic alcohols have been achieved on Pd/GC catalyst, as shown in Table 2.

4. Conclusions

In the present work, we have developed an efficient palladium on graphene catalyst for the selective oxidation of aromatic alcohols to corresponding carbonyl compounds via ideal green process, i.e. under solvent-free conditions and with molecular oxygen

as oxidant. Typically, extremely high activity with TOF of 30,137 mol/h mol_{Pd} can be achieved in the aerobic oxidation of benzyl alcohol to benzaldehyde using Pd/graphene as catalyst. The Pd/graphene catalyst shows good recyclability and no palladium leaching can be observed during reaction, which demonstrates its potential for industrial application.

The TEM and XPS results confirm that the catalytically-active palladium species exist in a quite similar state, i.e. particle sizes and electronic structure, in palladium catalysts on different carbon

supports. The FTIR spectra reveal that the adsorption of reactant benzyl alcohol is distinctly promoted compared to that on Pd/AC and Pd/CNT, due to the formation of π -electron interaction between benzene skeleton and graphene. The O₂-TPD profiles reveal that the adsorption of oxygen on Pd/GC is distinctly promoted due to oxygen spill-over from palladium sites to the adjacent bridge sites of graphene. Therefore, the superior reactivity of Pd/graphene in the aerobic oxidation of aromatic alcohols should be attributed to the promotion role of graphene support in the adsorption of reactant alcohol and oxygen.

Acknowledgments

This work is financially supported by the National Basic Research Program of China (2009CB623502) and 111 project (B12015). The support from the Ministry of Education of China (NCET-11-0251) is also acknowledged.

References

- [1] R.A. Sheldon, I.W.C.E. Arends, A. Dijkman, *Catalysis Today* 57 (2000) 157–166.
- [2] R.A. Sheldon, I.W.C.E. Arends, G.J. Ten Brink, A. Dijkman, *Accounts of Chemical Research* 35 (2002) 774–781.
- [3] T. Mallat, A. Baiker, *Chemical Reviews* 104 (2004) 3037–3058.
- [4] K. Mori, T. Hara, T. Mizugaki, K. Ebitani, K. Kaneda, *Journal of the American Chemical Society* 126 (2004) 10657–10666.
- [5] U.R. Pillai, E. Sahle-Demessie, *Green Chemistry* 6 (2004) 161–165.
- [6] M.S. Kwon, N. Kim, C.M. Park, J.S. Lee, K.Y. Kang, J. Park, *Organic Letters* 7 (2005) 1077–1079.
- [7] A.F. Lee, S.F.J. Hackett, J.S.J. Hargreaves, K. Wilson, *Green Chemistry* 8 (2006) 549–555.
- [8] J.D. Grunwaldt, M. Caravati, A. Baiker, *Journal of Physical Chemistry B* 110 (2006) 25586–25589.
- [9] S.F.J. Hackett, R.M. Brydson, M.H. Gass, I. Harvey, A.D. Newman, K. Wilson, A.F. Lee, *Angewandte Chemie International Edition* 46 (2007) 8593–8596.
- [10] T. Harada, S. Ikeda, M. Miyazaki, T. Sakata, H. Mori, M. Matsumura, *Journal of Molecular Catalysis A* 268 (2007) 59–64.
- [11] J. Chen, Q.H. Zhang, Y. Wang, H.L. Wan, *Advanced Synthesis and Catalysis* 350 (2008) 453–464.
- [12] H. Wang, S.X. Deng, Z.R. Shen, J.G. Wang, D.T. Ding, T.H. Chen, *Green Chemistry* 11 (2009) 1499–1502.
- [13] O.P. Tkachenko, L.M. Kustov, A.L. Tarasov, K.V. Klementiev, N. Kumar, D.Yu. Murzin, *Applied Catalysis A* 359 (2009) 144–150.
- [14] Y. Chen, Z. Guo, T. Chen, Y. Yang, *Journal of Catalysis* 275 (2010) 11–24.
- [15] T. Harada, S. Ikeda, F. Hashimoto, T. Sakata, K. Ikeue, T. Torimoto, M. Matsumura, *Langmuir* 26 (2010) 17720–17725.
- [16] A. Villa, D. Wang, N. Dimitratos, D. Su, V. Trevisan, L. Prati, *Catalysis Today* 150 (2010) 8–15.
- [17] K. Layek, H. Maheswaran, R. Arundhathi, M. Lakshmi Kantam, S.K. Bhargava, *Advanced Synthesis and Catalysis* 353 (2011) 606–616.
- [18] C.M.A. Parlett, D.W. Bruce, N.S. Hondow, A.F. Lee, K. Wilson, *ACS Catalysis* 1 (2011) 636–640.
- [19] X. Wang, G. Wu, N. Guan, L. Li, *Applied Catalysis B* 115–116 (2012) 7–15.
- [20] P. Serp, J.L. Figueiredo, *Carbon Materials for Catalysis*, John Wiley & Sons, Chichester, 2008.
- [21] K.S. Novoselov, A.K. Geim, S.V. Morozov, D. Jiang, Y. Zhang, S.V. Dubonos, I.V. Grigorieva, A.A. Firsov, *Science* 306 (2004) 666–669.
- [22] S. Stankovich, D.A. Dikin, G.H.B. Dommett, K.M. Kohlhaas, E.J. Zimney, E.A. Stach, R.D. Piner, S.T. Nguyen, R.S. Ruoff, *Nature* 442 (2006) 282–286.
- [23] A.K. Geim, K.S. Novoselov, *Nature Materials* 6 (2007) 183–191.
- [24] M.J. Allen, V.C. Tung, R.B. Kaner, *Chemical Reviews* 110 (2010) 132–145.
- [25] Y. Zhu, S. Murali, W. Cai, X. Li, J.W. Suk, J.R. Potts, R.S. Ruoff, *Advanced Materials* 22 (2010) 3024–3006.
- [26] I.Y. Jeon, Y.R. Shin, G.J. Sohn, H.J. Choi, S.Y. Bae, J. Mahmood, S.M. Jung, J.M. Seo, M.J. Kim, D. Wook Chang, L. Dai, J.B. Baek, *Proceedings of the National Academy of Sciences of the United States of America* 109 (2012) 5588–5593.
- [27] P.V. Kamat, *Journal of Physical Chemistry Letters* 1 (2010) 520–527.
- [28] G.M. Scheuermann, L. Rumi, P. Steurer, W. Bannwarth, R. Mülhaupt, *Journal of the American Chemical Society* 131 (2009) 8262–8270.
- [29] Y.S. Chen, Y.P. Wu, B. Wang, Y.F. Ma, Y. Huang, N. Li, F. Zhang, *Nano Research* 3 (2010) 661–669.
- [30] A.R. Siamaki, A.E.R. Khder, V. Abdelsayed, M.S. El-Shall, B.F. Gupton, *Journal of Catalysis* 279 (2011) 1–11.
- [31] S. Moussa, A.R. Siamaki, B.F. Gupton, M.S. El-Shall, *ACS Catalysis* 2 (2012) 145–154.
- [32] Ö. Metin, E. Kayhan, S. Özkar, J.J. Schneider, *International Journal of Hydrogen Energy* 37 (2012) 8161–8169.
- [33] Y. Li, Y. Yu, J. Wang, J. Song, Q. Li, M. Dong, C. Liu, *Applied Catalysis B* 125 (2012) 189–196.
- [34] S. Moussa, V. Abdelsayed, M.S. El-Shall, *Chemical Physics Letters* 510 (2011) 179–184.
- [35] W.S. Hummers, R.E. Offeman, *Journal of the American Chemical Society* 80 (1958) 1339.
- [36] S.H. Joo, S.J. Choi, I. Oh, J. Kwak, Z. Liu, O. Terasaki, R. Ryoo, *Nature* 412 (2001) 169–172.
- [37] M.A. Pimenta, G. Dresselhaus, M.S. Dresselhaus, L.G. Cancado, A. Jorio, R. Saito, *Physical Chemistry Chemical Physics* 9 (2007) 1276–1290.
- [38] C. Casiraghi, A. Hartschuh, H. Qian, S. Piscanec, C. Georgi, A. Fasoli, K.S. Novoselov, D.M. Basko, A.C. Ferrari, *Nano Letters* 9 (2009) 1433–1441.
- [39] M. Terrones, W.K. Hsu, A. Schilder, H. Terrones, N. Grobert, J.P. Hare, Y.Q. Zhu, M. Schworer, K. Prassides, H.W. Kroto, D.R.M. Walton, *Applied Physics A* 66 (1998) 307–317.
- [40] L. Liu, Z. Liu, J. Yang, Z. Huang, Z. Liu, *Carbon* 45 (2007) 2836–2842.
- [41] K.S. Subrahmanyam, S.R.C. Vivekchand, A. Govindaraj, C.N.R. Rao, *Journal of Materials Chemistry* 18 (2000) 1517–1523.
- [42] I.A. Aksay, M.J. McAllister, J.L. Li, D.H. Adamson, H.C. Schniepp, A.A. Abdala, J. Liu, M. Herrera-Alonso, D.L. Milius, R. Car, R.K. Prud'homme, *Chemistry of Materials* 19 (2007) 4396–4404.
- [43] W.H. Lee, P.J. Reucroft, *Carbon* 37 (1999) 7–14.
- [44] K.A. Wepasnick, B.A. Smith, J.L. Bitter, D.H. Fairbrother, *Analytical and Bioanalytical Chemistry* 396 (2010) 1003–1014.
- [45] K. Zhang, B.T. Ang, L. Li Zhang, X.S. Zhao, J. Wu, *Journal of Materials Chemistry* 21 (2011) 2663–2670.
- [46] C.D. Wagner, W.M. Riggs, L.E. Davis, J.F. Moulder, G.E. Muilenberg, *Handbook of X-ray Photoelectron Spectroscopy: A Reference Book of Standard Data for use in X-ray Photoelectron Spectroscopy*, Perkin-Elmer, Eden-Prairie, MN, 1979.
- [47] J.L. Figueiredo, M.F.R. Pereira, M.M.A. Freitas, J.J.M. Orfao, *Carbon* 37 (1999) 1379–1389.
- [48] L.M. Gómez-Sainero, X.L. Seoane, J.L.G. Fierro, A. Arcoya, *Journal of Catalysis* 209 (2002) 279–288.
- [49] *The Sadtler Handbook of Infrared Spectra*, BIO-RAD Laboratories, Inc., Richmond, 1978.
- [50] J.A. Hinojosa, H.H. Kan, J.F. Weaver, *Journal of Physical Chemistry C* 112 (2008) 8324–8331.
- [51] K. Nakada, A. Ishii, *Solid State Communications* 151 (2011) 13–16.
- [52] L. Chen, A. Yelon, E. Sacher, *Journal of Physical Chemistry C* 115 (2011) 7896–7905.
- [53] R. DiCosimo, G.M. Whitesides, *Journal of Physical Chemistry* 93 (1989) 768–775.
- [54] H.E. van Dam, L.J. Wisse, H. van Bekkum, *Applied Catalysis* 61 (1990) 187–197.